Occluded Boundary Detection for Small-footprint Ground-borne LIDAR Point Cloud Guided by Last-echo

Zhipeng Cai(蔡志鹏), Cheng Wang(王程), *Member, IEEE,* Chenglu Wen(温程璐), *Member*, *IEEE* and Jonathan Li, *Senior Member*, *IEEE*

***Abstract*—Occluded boundary detection in a 3D point cloud is an indispensable preprocessing step for many applications, such as point cloud completion [2]. Meanwhile, existing methods do not have the ability of distinguishing the occluded and complete surface borders, such as the border of a sign board. To solve this problem, this letter presents an occluded boundary detection method for small-footprint LIDAR point clouds. The main novelty of this work is using the last-echo information for occluded boundary detection. The seed boundary (SB) points are subsequently detected using this last-echo information. Finally, the SB points are grown into neighboring points using the occluded boundary growth algorithm. To the best of our knowledge, this method is the first that uses the last-echo information to detect occluded boundaries. Experimental results with comparisons indicate the proposed method can accurately and efficiently detect the occluded boundary without contamination from the complete surface border. These advantages allow the proposed method to benefit further applications such as point cloud completion, as demonstrated in the application section.**

***Index Terms*—point cloud, LIDAR, occluded boundary detection, last-echo**

I. Introduction

THE development of 3D laser scanners provides convenient means to acquire real-world 3D point cloud data. Occlusion is a general and inevitable problem that generates shadow-liked missing regions in the point cloud during its acquisition. Further processing of point clouds such as object detection [3] and 3D reconstruction [2] is often affected by occlusion. Occlusion manipulations heavily depend on accurately detecting the occluded boundary. A major difficulty for occluded boundary detection is distinguishing the complete surface border from the occluded boundary. This letter aims to detect the occluded boundary points in a small-footprint ground-borne LIDAR point cloud.

In previous literature [4-8], researchers considered occlusion detection for 2D images. Nevertheless, 3D point clouds differ and are more complex than 2D images. Some literature focusing on similar topics has recently been published. Bendels and Gerhard [1] proposed a multi-clue filtering based hole detection method for 3D point clouds. Wang et al.[9] proposed an edge extraction method that merged 3D point clouds and 2D images. However, none considered distinguishing the occluded boundary from the complete surface border.

In airborne laser scanning point cloud, the large-footprint multi-echo information has already been used in applications such as vegetation filtering [10] and building extraction [11, 12]. However, due to the significant difference in the footprint size between the airborne and close range ground-borne LIDAR systems, the characteristics of the last-echo information is significantly different, and therefore, the processing method and the potential applications are also quite different.

In most airborne LIDAR systems, the footprint size of the scanner is large. The large-footprint airborne systems have 10-70m footprint diameter, and the small-footprint airborne systems have 0.2-3m footprint diameter, depending on flying height and beam divergence. Most of the previous applications are based on large-footprint systems. Small-footprint systems have considerable potential but do not have dedicated applications [13]. With such a large footprint, the last-echo point of airborne LiDAR systems is not suitable for detecting the accurate occluded boundary.

In the small-footprint ground-borne LiDAR systems, the footprint size is much smaller due to the short distance from the scanner to the target. For instance, RIEGL VZ-1000 and RIEGL VMX-450, the 100 meter footprint diameter is 0.03m [14].

Small-footprint multi-echo LIDAR systems provide accurate location of the entire backscattered signal for each emitted laser pulse. This multi-echo information from the backscattered

This work was supported by the National Science Foundation of China (Project No. 61371144). (Corresponding author: C. Wang.)

Z. Cai (e-mail:czptc2h@gmail.com) and C. Wang (e-mail: cwang@xmu.edu.cn) are with Fujian Key Laboratory of Sensing and Computing for Smart City, School of Information Science and Engineering, Xiamen University, Computer Science, Xiamen 361005, China.

C. Wen is with Fujian Key Laboratory of Sensing and Computing for Smart City, School of Information Science and Engineering, Xiamen University, Cognitive Science, Xiamen 361005, China (e-mail: clwen@xmu.edu.cn).

J. Li is with the Key Laboratory of Underwater Acoustic Communication and Marine Information Technology (Ministry of Education), School of Information Science and Engineering, Xiamen University, Xiamen 361005, China and also with the GeoSpatial Technology and Remote Sensing Laboratory, University of Waterloo, Waterloo, ON N2L 3G1, Canada (e-mail: Junli@xmu.edu.cn).

signal reflects the order for all targets scanned by the same laser pulse. The last-echo is the last detected echo from a reflected waveform of a laser pulse, in addition, only the reflection with multiple echoes are concerned, single-echo reflection does not have last-echo (Shown in Figure 1). In this paper, we propose an original way to make use of the close relationship between the last-echo information and occlusion. Indeed, the last-echo allows to reveal the location of the occluded boundary. This observation inspired us to generate the proposed method for detecting occluded boundaries.

The proposed method makes three main contributions: (1) To the best of our knowledge, we are the first to discover that small-footprint last-echo points are able to help indicating the location of the occluded boundary. Using this property, the occluded boundary is quickly detected even for large-scale real-world data. And the complete surface border can be distinguished from the occluded boundary using last-echo information. (2) Outliers near the occluded regions are quickly and precisely removed using the indication of last-echo information. (3) The occluded boundary growth algorithm increases the detection rate for the occluded boundary points.

II. METHODOLOGY

The workflow for the proposed method is shown in Figure 2. All SB points are first extracted using last-echo information to indicate the occluded region. With the problem of low density of SB points, an occluded boundary growth algorithm is then proposed to extract all the occluded boundary points.

A. SB Point Detection

There are many small-footprint LIDAR systems capable of acquiring last-echo information. However, the potential of this information has not yet been realized. The major problem with detecting occluded boundary is distinguishing the occluded boundary points from complete surface boundary points. Building a mathematical model for occlusion is difficult in 3D space. Therefore, we proposed a novel usage of last-echo information in small-footprint ground-borne LIDAR systems to precisely detect the occluded boundary.

In a small-footprint multi-echo LIDAR system, the scanner emits a laser pulse to scan the object and records all the backscattered signals of the same laser pulse. As shown in Figure 1(a), multiple echoes are generated when a laser pulse is incompletely blocked by the front object and illuminates objects behind it. As shown in Figure 1(b), the order for each echo is recorded according to the time the laser pulse hits the corresponding object. Therefore, multi-echo information reveals the order of different objects scanned by the same laser pulse. Of the generated multiple echo points, the last-echo points are the last hit by the laser pulse, and are occluded by the front objects. Thus, last-echo points indicate the location of occluded boundaries.

The last-echo information is provided by the commercial LIDAR systems, such as the RIEGL VZ-1000 and VMX-450 systems. We label all of the extracted last-echo points as SB points. Using this indication, the proposed method avoids

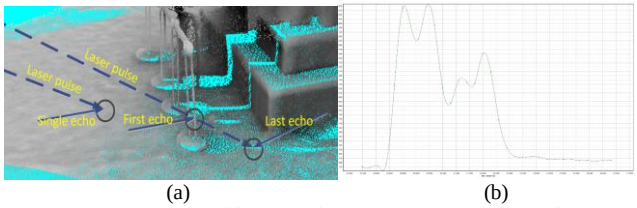

(a) (b)

Figure 1. Demonstration of full-waveform data and multi-echo information.

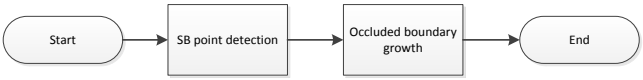

Figure 2. Workflow for the proposed method.

detecting the complete surface border which is not generated by the occlusion.

Due to the occlusion, the acquired coordinate accuracy for the last-echo points is not trustworthy. A LIDAR system uses the Time of Flight (ToF) principle to compute the distance between the laser scanner and target:

$$S = \frac{cn}{2f}, \tag{1}$$

where S is the distance to the target, c is the speed of light, n is the number of returned signals received by the sensor, and f is the frequency of the oscillator. When occlusion occurs, only part of the laser beam illuminates the target. Thus, some of the returned signal for the last-echo point may have lower intensity than the signal detection threshold, which lowers the measured n in equation (1) from the real number. Consequently, the measured distance to the target may be lower than the real distance, which produces the erroneous last-echo points. Therefore, the initially detected SB points usually include outliers (shown in Figure 3(a)). Additionally, when the returned signal disappears, no last-echo point will be detected. As a result, the density of SB points is usually low.

This phenomenon affects the performance of many applications, such as point cloud completion and reconstruction. Based on these observations, we propose an efficient, two-step outlier removal process: 1) remove all last-echo points; 2) find for each removed last-echo point a nearest point to be the new SB point. Figure 3(a) shows an occluded region filled with outliers. All of the blue points were the first detected SB points. Figure 3(b) shows the same region after removing all last-echo points and detecting new SB points (painted blue). In this way, most of the outliers were removed, and the occluded boundary

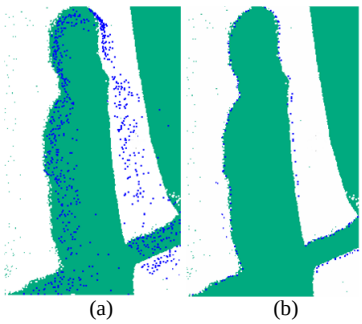

(a) (b)

Figure 3. Outlier removal. (a): Occluded region with outliers. (b): Occluded region after the outlier removal process. The blue points are the SB points.

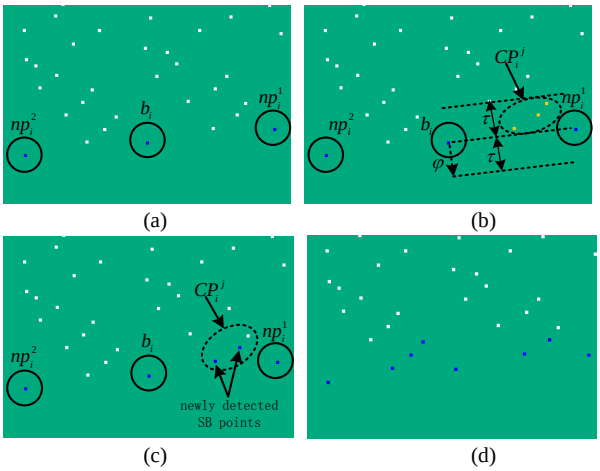

Figure 4. The occluded boundary growth algorithm. (a): The result of the SB point detection. (b): Extracting CP_i^1 between b_i and np_i^1. (c): The newly detected SB points between b_i and np_i^1. (d): The result of occluded boundary growth.

contour was accurately detected.

B. *Occluded Boundary Growth Algorithm*

The last-echo point density is usually low, which makes it difficult to precisely indicate the entire occluded boundary. Therefore, we propose an occluded boundary growth algorithm to enhance the detected boundary point density and benefit further applications.

The occluded boundary growth algorithm finds the undetected boundary points near each SB point. The occluded boundary growth algorithm for each SB point consists of three steps (shown in Figure 4):

1. For every SB point, b_i, find np_i^1 and np_i^2 which are the two SB points nearest and are on the opposite sides to b_i. If there are fewer than two points on the opposite sides of b_i within a certain radius, r, then find as many points as possible. r is defined as follows when P denotes the original point cloud:

$$r = 5 * \min_{p_i, p_j \in P} \| p_i - p_j \| (p_i \neq p_j), \tag{2}$$

specifically, the factor '5' in equation (2) was set according to our experience. It works well in our data acquired by the RIEGL VZ-1000 and VMX-450 system. The factor can be turned larger for other LIDAR systems to guarantee the ability of finding np_i^1 and np_i^2. And the time cost is not heavily affected by the adjustment of parameter r. The efficiency of the proposed method using different parameter r is shown in the discussion section. np_i^1 is defined as:

$$np_i^1 = \begin{cases} \arg\min_{b_j \neq b_i} (\| b_i - b_j \|), & (\min_{b_j \neq b_i} (\| b_i - b_j \|) \leq r) \\ \varnothing, & (\min_{b_j \neq b_i} (\| b_i - b_j \|) > r). \end{cases} \tag{3}$$

Let N_{bi} denote the neighbor point set for b_i within a radius r. Define:

$$\varphi = \frac{\sum_{p_j \in N_{bi}} (b_i - p_j)}{\| \sum_{p_j \in N_{bi}} (b_i - p_j) \|}, \tag{4}$$

which is the normalized mean vector from all the points of N_{bi} to b_i. np_i^2 is found if $\exists b_k \neq b_i$, such that:

$$(v_2 - v_2 \cdot \varphi \cdot \varphi) \cdot (v_1 - v_1 \cdot \varphi \cdot \varphi) < 0, \tag{5}$$

where $v_1 = np_i^1 - b_i$ and $v_2 = b_k - b_i$. Let B_2 denote all the SB points that meet the equation (4), then np_i^2 is defined as:

$$np_i^2 = \begin{cases} \arg\min_{b_k \in B_2} (\| b_k - b_i \|), & (\min_{b_k \in B_2} (\| b_i - b_k \|) \leq r) \\ \varnothing, & (\min_{b_k \in B_2} (\| b_i - b_k \|) > r). \end{cases} \tag{6}$$

2. For np_i^j, construct the boundary extension line segment l_i^j and if $\| l_i^j \| > \frac{r}{2}$, extract all points within a distance , τ, from l_i^j, where:

$$\tau = \frac{\sum_{p_j \in N_{bi}} \min_{p_k \neq p_j, p_k \in N_{bi}} \| p_j - p_k \|}{| N_{bi} |}. \tag{7}$$

Using τ as a bounding radius reduces the time cost for the next step. The extracted points are defined by the point set CP_i^j.

3. Detect all boundary points within CP_i^j using the feature proposed by Bendels [1]. The feature for boundary detection contains three parts: 1) the angle criterion, 2) the halfdisc criterion and 3) the shape criterion.

The effect of the occluded boundary growth algorithm is demonstrated in the next section.

III. Experimental Results

The experimental test for the proposed method used real-world point cloud data acquired by a RIEGLVZ-1000 system and a RIEGL VMX-450[1] system. Other kinds of laser scanning systems are also able to provide last-echo information such as all other RIEGL VZ-Series systems. The proposed method was implemented using C++ and executed on a computer with an Intel Core(TM) i3-2120 3.30GHz CPU, and 4.0 GB RAM.

A. *Results & Discussion*

The result for the proposed method is shown in Figure 5. The occluded boundary points were precisely detected under various occlusion situations. Because the last-echo will not be generated on the complete surface border, complete surface border points (like boundary points of the window in Figure 5(a) and the window of a car in Figure 5(f)) are perfectly excluded. The density of the boundary points is sufficiently high to provide information for further applications.

1. Our laser scanning system can be found at http://www.riegl.com/

The time cost of the proposed method is shown in Table 1 of the comparison section. For all demonstrated large scale real-world point clouds, the proposed method was fast.

The efficiency of the proposed method is not heavily related to the parameter r. Figure 6 shows the effect of parameter r had on the time cost for four point cloud data. The time cost remained nearly unchanged after increasing r.

The effect of the occluded boundary growth algorithm is shown in figure 7. Before the execution of the algorithm, there remain undetected occluded boundary points between each pair of SB points (shown in Figure 7(a)). In contrast, after the occluded boundary growth, most of the undetected occluded boundary points between two SB points are detected (shown in Figure 7(b)).

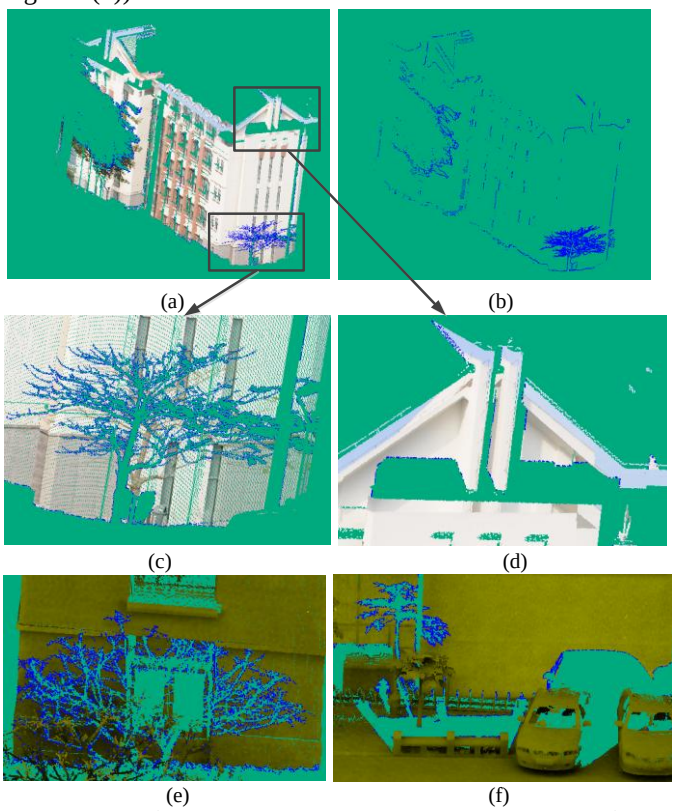

Figure 5. Results from the proposed method. (a): The detection result of the entire data. (b): Detected occluded boundary points. (c)&(d): Partially enlarged detail of (a). (e)&(f): Other data with different occlusion situations. The blue points are detected occluded boundary points.

B. *Comparison*

In this section, we compare the performance for the proposed method to the method of Bendels and Gerhard [1]. As shown in Figure 8, within the two large-scale real-world data, the method of Bendels and Gerhard cannot distinguish the occluded boundary from the complete surface border. The boundary of window frames and the edge of walls which are all complete surface borders, are not excluded in Figure 8(a) and Figure 8(c). In contrast, the proposed method can not only precisely detect the occluded boundary points, but also perfectly exclude the complete surface border.

The time cost and accuracy of the two methods are shown respectively in Table 1 and Table 2. In Table 2, the Tpr refers to the true positive rate, and the Fpr refers to the false positive rate.

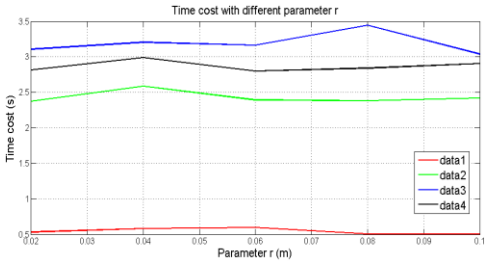

Figure 6. Time cost for the proposed method with different parameter r.

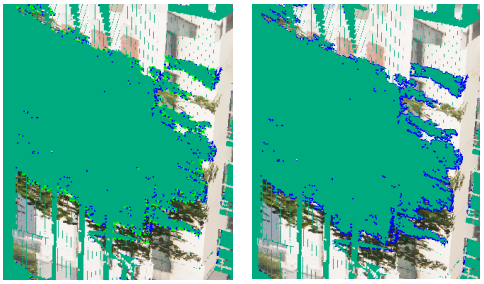

Figure 7. The result of occluded boundary growth algorithm. (a): The result before the execution of the algorithm. (b): The result after the execution of the algorithm. The blue points are detected occluded boundary points.

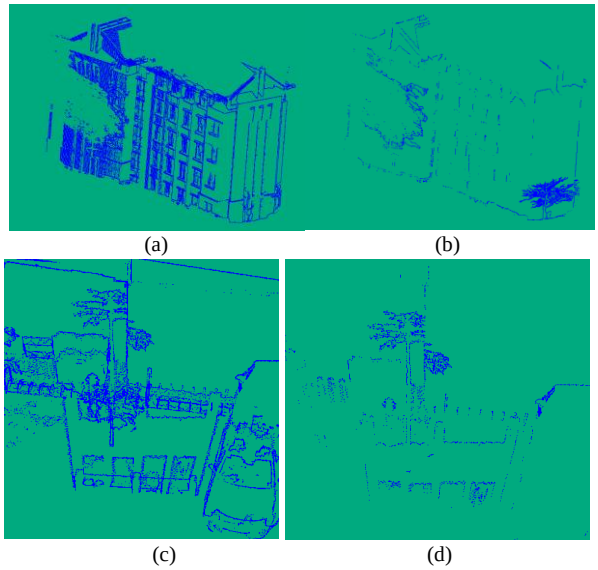

Figure 8. Comparative results. Left: The result for Bendels and Gerhard. Right: The result using the proposed method.

Data	number of points	time cost of Bendels and Gerhard [1] (s)	time cost of the proposed method (s)	Time reduction rate
Data 1	815374	30.830	0.360	98.83%
Data 2	6175412	3503.900	1.407	99.96%
Data 3	12031293	11417.700	2.521	99.98%

Table 1. Time cost of the proposed method and the method of Bendels and Gerhard.

Result of the proposed method	Tpr of our method	Fpr of our method	Tpr by [1]	Fpr by [1]
Data 4	99.21%	0	26.33%	5.34%
Data 5	96.85%	0	1	28.63%
Data 6	98.15%	0	1	6.13%

Table 2. Accuracy measurements of the detection result.

The proposed method utilizes last-echo information to quickly locate the occluded region. Therefore, the proposed method significantly reduces the time cost for calculating the complex

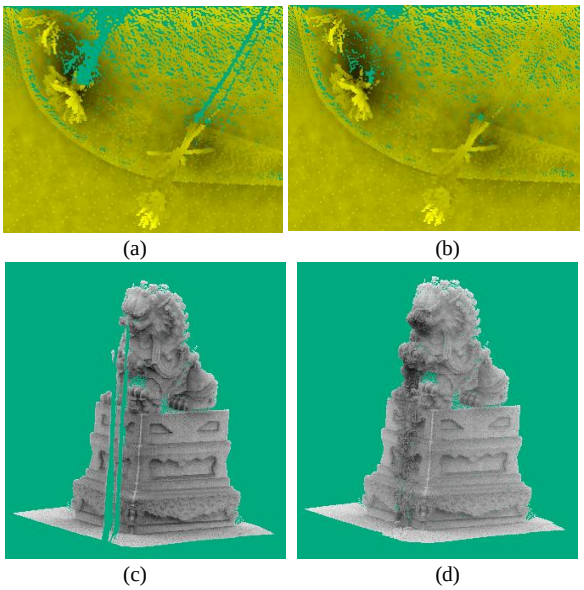

Figure 9. Application of point cloud completion. Left: Original data with occlusion. Right: Completion results using the proposed method.

geometric feature throughout all points of the data. When the number of points exceeded 12 million, the method of Bendels and Gerhard cost more than 3 hours. In contrast, the proposed method cost only 2.521 seconds, which is about 500 times faster than the method of Bendels and Gerhard.

For accuracy measurements, we manually selected all occluded boundary points to define the ground truth because no standard database for occluded boundary detection in point cloud exists. And in the experiment, a ground truth point is considered correctly detected if there is at least one detected occluded boundary point within a certain distance (0.03m in practice) of the ground truth point. The proposed method yielded a true positive rate above 96% with no false positive points because last echo information provides the capability to extract only occluded boundary points. In contrast, the method of Bendels was sensitive to the density of the neighbor points, and unstable for data with different density levels. In Data 4, which is the data in Figure 5(a), many thin gaps on the wall occluded by the tree branches were not detected by the method of Bendels, which caused the low true positive rate. For all of the data, the fpr of the method of Bendels was higher than 5% (28.63% for Data 5), which is intolerable because all data has more than 50000 points. Thus, there were always over 2500 false detected points, which will lead to unacceptable errors in further applications.

C. *Further Study on Point Cloud Completion*

The proposed method is able to benefit further applications. Here, we implemented the point cloud completion application which is shown in Figure 9. We first used the proposed method to accurately detect the occluded boundaries, and then completed the occluded regions based on the occluded boundaries. In Figure 9(b) and 9(d), all of the incomplete regions were perfectly completed.

IV. CONCLUSION

This letter presented a novel, last-echo-based occluded boundary detection method for small-footprint ground-borne LIDAR point clouds. First, innovative use of guidance from last-echo information allowed the location of the occluded boundary to be quickly and precisely detected through the SB point detection procedure. Outliers near the occluded boundary were precisely removed via an efficient outlier removal process during the SB point detection. The complete surface borders were excluded from the occluded boundary using last-echo information. The occluded boundary growth algorithm then increased the detection rate of the occluded boundary points. The results from the discussion and comparison reveal the advantages of the proposed method: 1) high accuracy, 2) low time cost and 3) the ability to distinguish the occluded boundary from the complete surface border. Occlusions in structures like tree leaves are not specially removed, which may be a limitation for further applications.

REFERENCES

[1] G. H. Bendels, "Detecting holes in point set surfaces," 2006.

[2] A.-L. Chauve, P. Labatut, and J.-P. Pons, "Robust piecewise-planar 3D reconstruction and completion from large-scale unstructured point data," in *Computer Vision and Pattern Recognition (CVPR), 2010 IEEE Conference on*, 2010, pp. 1261-1268.

[3] H. Wang, C. Wang, H. Luo, P. Li, M. Cheng, C. Wen, *et al.*, "Object Detection in Terrestrial Laser Scanning Point Clouds Based on Hough Forest," 2014.

[4] Y. Xu, L. Qin, G. Li, and Q. Huang, "An efficient occlusion detection method to improve object trackers," in *ICIP*, 2013, pp. 2445-2449.

[5] A. Ayvaci, M. Raptis, and S. Soatto, "Occlusion detection and motion estimation with convex optimization," in *Advances in neural information processing systems*, 2010, pp. 100-108.

[6] D. Sun, C. Liu, and H. Pfister, "Local layering for joint motion estimation and occlusion detection," in *Computer Vision and Pattern Recognition (CVPR), 2014 IEEE Conference on*, 2014, pp. 1098-1105.

[7] A. N. Stein and M. Hebert, "Occlusion boundaries from motion: Low-level detection and mid-level reasoning," *International journal of computer vision*, vol. 82, pp. 325-357, 2009.

[8] P. Sundberg, T. Brox, M. Maire, P. Arbeláez, and J. Malik, "Occlusion boundary detection and figure/ground assignment from optical flow," in *Computer Vision and Pattern Recognition (CVPR), 2011 IEEE Conference on*, 2011, pp. 2233-2240.

[9] Y. Wang, D. Ewert, D. Schilberg, and S. Jeschke, "Edge extraction by merging 3D point cloud and 2D image data," in *Emerging Technologies for a Smarter World (CEWIT), 2013 10th International Conference and Expo on*, 2013, pp. 1-6.

[10] G. Vosselman and H.-g. Maas, "Adjustment and filtering of raw laser altimetry data," in *Proceedings of OEEPE Workshop on Airborne Laserscanning and Interferometric SAR for Detailed Digital Terrain Models, Stockholm, Sweden*, 2001.

[11] G. Zhou and X. Zhou, "Seamless Fusion of LiDAR and Aerial Imagery for Building Extraction," 2014.

[12] G. Zhou, C. Song, J. Simmers, and P. Cheng, "Urban 3D GIS from LiDAR and digital aerial images," *Computers & Geosciences*, vol. 30, pp. 345-353, 2004.

[13] C. Mallet and F. Bretar, "Full-waveform topographic lidar: State-of-the-art," *ISPRS Journal of photogrammetry and remote sensing*, vol. 64, pp. 1-16, 2009.

[14] J. L. Carrivick, M. W. Smith, and D. M. Carrivick, "Terrestrial laser scanning to deliver high-resolution topography of the upper Tarfala valley, arctic Sweden," *GFF*, pp. 1-14, 2015.